analytical chemistry

pubs.acs.org/ac Article

In Situ Translation of Terminal Glycans into Covalent Readouts in Complex Biological Systems

Haiqi Wang,△ Ru Jia,△ Junpeng Xu, Qi Li, Yiran Li, Yunyan Yao, Ruiyuan Wang, Xincheng Kong, Yu Zhu, Chao Yan, Jian He,* Pengchao Li,* Lin Ding,* and Huangxian Ju

Cite This: *Anal. Chem.* 2026, 98, 20531−20541 Read Online

ACCESS | Metrics & More | Article Recommendations | Supporting Information

ABSTRACT: Glycans exhibit pronounced spatial heterogeneity in tissues and organs. However, glycan detection in these complex biological systems remains challenged by strong background interference, limited labeling efficiency, and difficulty in faithfully preserving spatial information. To address these issues, we developed a reduction-assisted galactose oxidase labeling platform (ReGOL). By introducing $NaBH_4$ prereduction to suppress fixation-derived background and integrating galactose oxidase oxidation with fast hydrazone ligation into an efficient readout workflow, ReGOL enables high-fidelity imaging of terminal galactose/*N*-acetylgalactosamine (Gal/GalNAc) in tissue sections. The method is applicable to both frozen and paraffin-embedded sections and can be sequentially combined with hematoxylin and eosin (H&E) staining on the same section, allowing direct correlation between glycan signals and histological structures. In addition, we established a neuraminidase-ReGOL versus ReGOL comparative strategy to distinguish exposed terminal Gal/GalNAc from sialic acid-capped counterparts, and applied it to analyze changes in terminal glycan spatial distribution and glomerular morphology in a renal fibrosis model. In a bladder cancer model, ReGOL clearly delineated the tumor−peritumoral-urothelium boundary and revealed tumor-associated glycan heterogeneity. Building on this, we further translated the 15 min labeling workflow to the bladder in vivo, enabling selective glycan imaging of tumor regions. This system also enabled selective installation of bioorthogonal chemical handles onto the glycocalyx of bladder tumors in vivo, thereby supporting subsequent chemical functionalization. Collectively, this work establishes an oxidation-based glycan analysis platform applicable to both tissue sections and living systems, and provides a practical method for spatial analysis and localized chemical intervention of terminal glycans in complex biological environments.

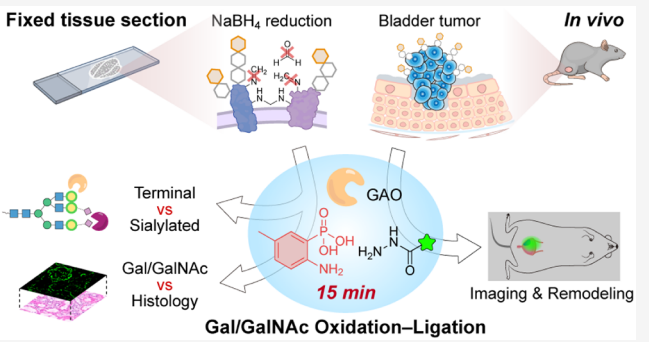

Downloaded via NANJING UNIV on July 16, 2026 at 15:46:04 (UTC).
See https://pubs.acs.org/sharingguidelines for options on how to legitimately share published articles.

Glycans are structurally diverse and dynamically regulated biomolecules across multiple biological scales, from cells to tissues and organs.[1−3] In tissue and organ contexts, their spatial heterogeneity is closely associated with tissue architecture, cellular states, and disease-associated remodeling,[4] and is increasingly recognized as a feature of pathological progression, including fibrosis and cancer.[5,6] Despite major advances in glycan labeling and imaging,[7,8] reliable glycan detection in complex biological systems, such as tissue sections and living organisms, remains challenging. This difficulty arises from the structural complexity and spatial heterogeneity of glycans, the lack of universal high-specificity recognition tools, and the challenge of interpreting glycan readouts within histologically complex biological contexts.[9,10]

For conventional tissue sections, metabolic glycan labeling is generally not applicable because it depends on active precursor uptake and intracellular biosynthetic metabolism.[11] Accordingly, extracellular recognition-based and chemoenzymatic labeling strategies have become more practical for histological glycan analysis. Lectin-based histochemistry is simple and widely used,[12,13] but its motif-level recognition and frequent cross-reactivity often limit structural specificity.[14,15] By contrast, chemoenzymatic labeling offers improved selectivity and has been applied to tissue specimens, as exemplified by ST3Gal1- and ST6Gal1-based labeling for glycan detection.[16] However, glycosyltransferase-based methods still face practical limitations in complex samples, including restricted catalytic efficiency, the cost and synthetic burden of modified sugar-nucleotide donors, and a bias toward selected acceptor motifs rather than broad coverage of terminal glycan epitopes.[17]

A complementary strategy is to convert native terminal glycans into chemically addressable handles. In this context, galactose oxidase (GAO) selectively oxidizes terminal galactose/*N*-acetylgalactosamine (Gal/GalNAc) residues to

Received: April 8, 2026
Revised: June 23, 2026
Accepted: June 24, 2026
Published: June 30, 2026

ACS Publications © 2026 American Chemical Society

https://doi.org/10.1021/acs.analchem.6c02366
Anal. Chem. 2026, 98, 20531−20541

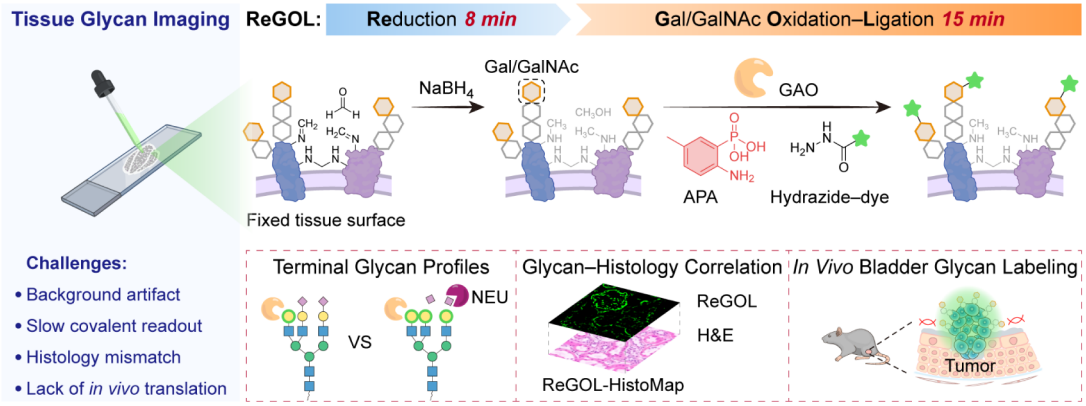

Figure 1. Schematic of the ReGOL/GOL strategy for high-fidelity tissue glycan imaging. Gal/GalNAc, galactose/*N*-acetylgalactosamine; GAO, galactose oxidase; APA, (2-amino-5-methylphenyl)phosphonic acid; NEU, neuraminidase.

aldehydes,[18] providing a covalent entry point for subsequent hydrazone or oxime ligation. Importantly, Gal/GalNAc may occur either as exposed terminal epitopes or as penultimate residues masked by sialic acid (Sia).[19] Thus, when combined with neuraminidase (NEU) pretreatment,[20] the GAO-based platform can access both exposed terminal Gal/GalNAc and Sia-capped Gal/GalNAc, thereby covering two major modes of terminal glycan presentation.[21] However, in complex biological settings, the performance of such oxidation−ligation workflows can still be compromised by endogenous aldehyde- and Schiff base-related backgrounds[22] and by the relatively slow kinetics of aldehyde-based ligation under biocompatible conditions.[23] Therefore, improved strategies are needed to preserve glycan information with high fidelity in situ. Extending such a system to living animals would further enable direct visualization of native glycan states in intact physiological environments,[7,24] thereby opening opportunities for dynamic disease monitoring and localized glycan intervention.[25,26]

Herein, we developed a Gal/GalNAc labeling strategy for high-fidelity imaging of terminal glycans in tissue sections and living bladders (Figure 1). A $NaBH_4$ prereduction step was introduced to suppress fixation-derived background in tissue sections. Subsequently, a one-step Gal/GalNAc Oxidation−Ligation (GOL) workflow was employed: terminal Gal/GalNAc residues were oxidized by GAO and underwent efficient hydrazone ligation catalyzed by (2-amino-5-methylphenyl)phosphonic acid (APA). Together, these steps constitute a rapid and operationally simple platform, termed "Reduction → Gal/GalNAc Oxidation−Ligation" (ReGOL), for tissue glycan analysis. We demonstrate that ReGOL is compatible with both frozen and paraffin-embedded sections, supports same-section correlation of glycan signals with histological information, and can be combined with neuraminidase pretreatment (NEU-ReGOL) to resolve Sia-capped Gal/GalNAc from terminal Gal/GalNAc. Using normal tissues and disease models, we show that this platform enables spatially resolved analysis of terminal glycan patterns in the kidney and at bladder tumor boundaries. Furthermore, we translate the 15 min GOL workflow to the living bladder for in vivo glycan imaging and localized chemical remodeling. Together, these results establish a practical oxidation-based strategy for tissue and in vivo glycan analysis, and extend glycan imaging from ex vivo histology toward localized chemical interrogation in living systems.

METHODS

Animals

C57BL/6 female mice, aged 6−8 weeks, were obtained from SPF Biotechnology Co., Ltd. (Beijing, China) and maintained under specific pathogen-free conditions. Mice were housed in a room at 20−22 °C and 50−60% humidity with free access to standard rodent chow and water. Mice were euthanized by CO_2 inhalation at the end of the experiments. All animal experiments were approved by the Nanjing University Institutional Animal Care and Use Committee (IACUC-2310002).

Unilateral Ureteral Obstruction (UUO) Model

Mice were anesthetized with isoflurane and placed in a supine position. A left flank incision of 1−1.5 cm was made to expose the left kidney and ureter. The left ureter was ligated at two points using 4−0 silk sutures. The kidney was repositioned and the muscle and skin were sutured layer by layer. Mice were returned to their cages and monitored daily. On postoperative day 14, UUO and contralateral unobstructed (CU) kidneys were collected, decapsulated, and washed with PBS for subsequent tissue sectioning.

Orthotopic Bladder Cancer Model

MB49-luc cell suspension was prepared at a concentration of 2×10^7 cells/mL in PBS. Mice were anesthetized with tribromoethanol. An IV Catheter (24 G × 0.75 in., BD Insyte, 381212) was gently inserted into the mouse bladder through the urethra for intravesical instillation. Residual urine in the bladder was removed by applying gentle pressure. $AgNO_3$ (0.3 M, 5 μL) was first injected intravesically for 20 s to induce urothelial injury, followed by intravesical instillation of 50 μL of MB49-luc cell suspension. Mice were returned to their cages after 2 h. Ten days after tumor inoculation, mice were injected intraperitoneally with D-luciferin sodium salt and examined by bioluminescence imaging using an IVIS system to confirm tumor formation.

ReGOL-Related Experiments

Standard ReGOL. Tissue sections were incubated with a reducing solution (PBS containing 10 mg/mL $NaBH_4$) at room temperature for 8 min to quench residual aldehyde and Schiff base groups, followed by thorough washing with PBS. The sections were then incubated with a GOL solution (PBS containing 100 μg/mL GAO, 10 mM APA, 50 μM AF488-Hz or AF647-Hz, and 10 mg/mL BSA) at 37 °C for 15 min for Gal/GalNAc labeling. After washing with PBS, the sections were mounted with antifade mounting medium (with DAPI). Images were acquired using a confocal laser scanning microscopy (CLSM) or a whole-slide scanner.

ReGOL-Histomap. Following execution of the standard ReGOL procedure on tissue sections, fluorescence images were acquired using a whole-slide scanner. Coverslips were then gently removed in water, and the sections were washed thoroughly to remove mounting

https://doi.org/10.1021/acs.analchem.6c02366
Anal. Chem. 2026, 98, 20531−20541

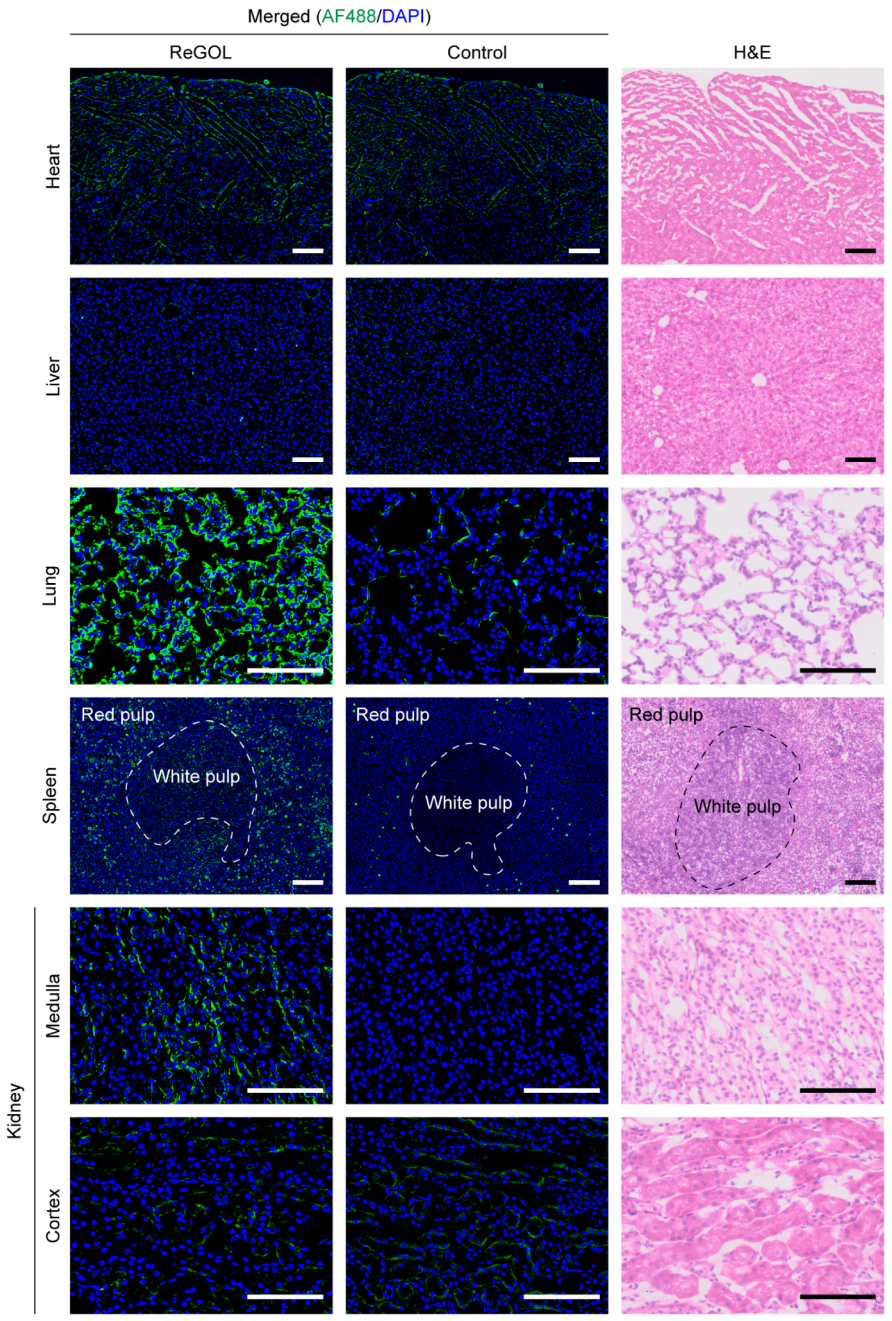

Figure 2. Scanned images of frozen sections from five major organs (heart, liver, lung, spleen, and kidney) of normal mice after ReGOL (using AF488-Hz as the hydrazide probe), control treatment (omitting GAO), or H&E staining. Whole-slide images are shown in Figure S7. AF488, labeling signal; DAPI, nuclei. Scale bars: 100 μm. n = 3 for each group.

medium. The sections were subsequently subjected to standard H&E staining, mounted with neutral mounting medium, and scanned again using the whole-slide scanner.

NEU-ReGOL. Tissue sections were incubated with a NEU-containing solution (200 U/mL α2−3,6,8,9 Neuraminidase A in PBS, pH 5.5) at 37 °C for 3 h, followed by thorough washing with PBS. The sections were then subjected to the standard ReGOL procedure.

Images were analyzed using ImageJ (version 1.54k). The area and number of visually identifiable individual glomeruli were quantified, and morphological parameters, including circularity, aspect ratio, and solidity, were further analyzed. The cortical region was defined by referring to adjacent tissue sections stained with Masson's trichrome, followed by area quantification using ImageJ.

In Vivo Imaging of Bladder Glycans Using GOL

Ten days after tumor inoculation, mice with confirmed tumors were randomly divided into two groups. Normal mice were also randomly divided into two groups for comparison. After anesthesia, the mouse bladders were rinsed intravesically with PBS, instilled with 50 μL of GOL solution (PBS containing 100 μg/mL GAO, 10 mM APA, 50 μM IR783-Hz, and 10 mg/mL BSA). GAO and APA were omitted in control groups. After 15 min, the bladders were rinsed intravesically with PBS. Then, in vivo fluorescence signals were collected using the IVIS system.

To quantify fluorescence intensity, all bladders were harvested, arranged by group, and imaged ex vivo using the IVIS system.

https://doi.org/10.1021/acs.analchem.6c02366
Anal. Chem. 2026, 98, 20531−20541

In Vivo Chemical Remodeling of Bladder Glycans Using GOL

To prepare the heterobifunctional probe TCO-Hz containing *trans*-cyclooctene (TCO) and hydrazide (Hz) groups, a PBS solution containing 7.5 mM TCO-PEG_4-DBCO and 5 mM azido-PEG_4-hydrazide was stirred at 37 °C for 3 h. The reaction was considered nearly complete, yielding ∼5 mM TCO-Hz. The mixture was used directly in the subsequent animal experiments.

Ten days after tumor inoculation, mice with confirmed tumors were randomly divided into two groups. Normal mice were also randomly divided into two groups for comparison. After anesthesia, the mouse bladders were rinsed intravesically with PBS, instilled with 50 μL GOL solution (PBS containing 100 μg/mL GAO, 10 mM APA, 50 μM TCO-Hz, and 10 mg/mL BSA). GAO and APA were omitted in control groups. After 15 min, the bladders were rinsed intravesically with PBS.

To visualize TCO installation, frozen sections obtained from the bladders in each group were blocked with 10 mg/mL BSA at 4 °C for 1 h, stained with 0.5 μM Tz-Cy5 at 4 °C for 30 min, and then mounted with antifade mounting medium (with DAPI). CLSM images were captured using a 20× objective.

RESULTS AND DISCUSSION

GOL Enables High-Efficiency Cellular Glycan Imaging

Our group has previously demonstrated that APA catalyzes hydrazone ligation more efficiently than the conventional catalyst aniline (AN) while remaining compatible with live-cell systems.[27] In the present study, considering the specific demands of glycan labeling on tissue sections and in vivo, including suppression of fixation-derived background, rapid covalent readout under biocompatible conditions, and a streamlined workflow, we combined GAO oxidation and APA-catalyzed hydrazone ligation into a single-step procedure ("GOL"), in which GAO continuously generates aldehydes that are immediately captured by the hydrazide probe.

The feasibility of GOL was first validated in solution prior to cellular studies. Methyl α-D-galactopyranoside (MeGal) was employed as a model substrate to mimic terminal galactose residues on the cell surface, while fluorescein-5-thiosemicarbazide (FTZ) served as a hydrazide analogue labeling probe (Figure S1a). As revealed by high-performance liquid chromatography (HPLC) and high-resolution mass spectrometry (HRMS), MeGal was almost completely converted to the corresponding MeGal-FTZ product under the reaction conditions (Figure S1b).

To evaluate the performance of this GOL strategy on cells, mouse bladder carcinoma MB49 cells and mouse fibroblast L929 cells, which display distinct cell-surface Gal/GalNAc densities,[27] were employed as a simplified model pair representing different cellular glycosylation states encountered in tissues. We characterized the kinetics of GOL in these cell types using APA or AN as the catalyst (denoted by GOL(APA) and GOL(AN), respectively) and Alexa Fluor 488 hydrazide (AF488-Hz) as the hydrazide probe. Given that hydrazone hydrolysis under physiological conditions (PBS, pH 7.4) occurs on a time scale of hours,[28] it is expected to be negligible within the analytical time window. As quantified by the mean fluorescence intensity per pixel in the cell membrane (FI_m) from confocal images, the signals of both GOL(APA) and GOL(AN) increased continuously over 1 h (Figure S2a,b), consistent with a consecutive unimolecular reaction model.[29] GOL(APA) consistently produced stronger signals than GOL(AN) and more effectively amplified the signal difference (ΔFI_m) between the two cell types (Figure S2c). Notably, clear visual discrimination between the two cell types was already achieved after 15 min of GOL(APA) treatment (Figure S2a). On this basis, 15 min was adopted as a practical working condition for the subsequent tissue glycan labeling experiments.

ReGOL Enables High-Fidelity Tissue Glycan Imaging

To preserve tissue morphology and cellular architecture, tissue samples are typically fixed with aldehyde-based fixatives such as paraformaldehyde or formalin before sectioning. However, residual aldehydes and Schiff base-related species generated during fixation can contribute to background fluorescence[22] and interfere with subsequent hydrazone/oxime ligation. We therefore introduced a $NaBH_4$ reduction step before GOL (termed "ReGOL"). Using frozen sections from different organs, we confirmed the necessity of this step: $NaBH_4$ treatment effectively suppressed endogenous interfering signals (Figures S3−S5) and improved the signal-to-background ratio (SBR) (Figure S6), whereas omission of $NaBH_4$ led to pronounced nonspecific fluorescence that would compromise accurate evaluation of glycan abundance and spatial distribution.

We next validated ReGOL in frozen sections from five major organs of normal mice, including heart, liver, lung, spleen, and kidney. Distinct fluorescence intensities and spatial distribution patterns were observed across these organs (Figures 2, S7). Control groups showed negligible signals, further confirming that $NaBH_4$ efficiently minimized background. Comparative analysis indicated that Gal/GalNAc labeling was lowest in the heart and liver, highest in the lung, and intermediate in the spleen and kidney. Among these tissues, the spleen and kidney exhibited particularly notable spatial heterogeneity. In the spleen, the signal was concentrated in the red pulp and sharply demarcated from the white pulp. This pattern highlights the ability of ReGOL to resolve glycan heterogeneity at the level of splenic microanatomical compartments. In the kidney, medullary signals displayed axially aligned patterns, possibly corresponding to renal tubular structures, whereas cortical signals remained close to the control level, suggesting limited labeling specificity in the cortex under the present conditions. We also performed lectin staining targeting Gal/GalNAc-containing motifs on kidney sections (Figure S8). *Erythrina cristagalli* lectin (ECL) and soybean agglutinin (SBA) displayed a similar striated pattern in the medulla, supporting the presence of regional differences in glycan distribution within the kidney. Although apparent tubular staining was observed in the cortex, comparison with ReGOL labeling suggests that this signal may be partially influenced by nonspecific adsorption of fluorescein.

To validate that ReGOL labeling signals reflect terminal Gal/GalNAc abundance, we employed a galactose polymer (pGal) conjugated with Cy5 and 1,2-distearoyl-*sn*-glycero-3-phosphoethanolamine (DSPE), termed Cy5-pGal-DSPE. This probe introduces defined galactose residues into tissues, with Cy5 fluorescence providing an independent readout of probe abundance and spatial distribution. As shown in Figure S9, in heart and liver tissues that originally exhibited low endogenous ReGOL signals, the Cy5 distribution pattern observed after probe insertion closely overlapped with the ReGOL labeling pattern. Notably, the ReGOL signals correlated with the Cy5 signals (Figure S10a), and the ratios of newly generated ReGOL signals to Cy5 signals were comparable between the two tissues (Figure S10b), indicating that ReGOL reflects

https://doi.org/10.1021/acs.analchem.6c02366
Anal. Chem. 2026, 98, 20531−20541

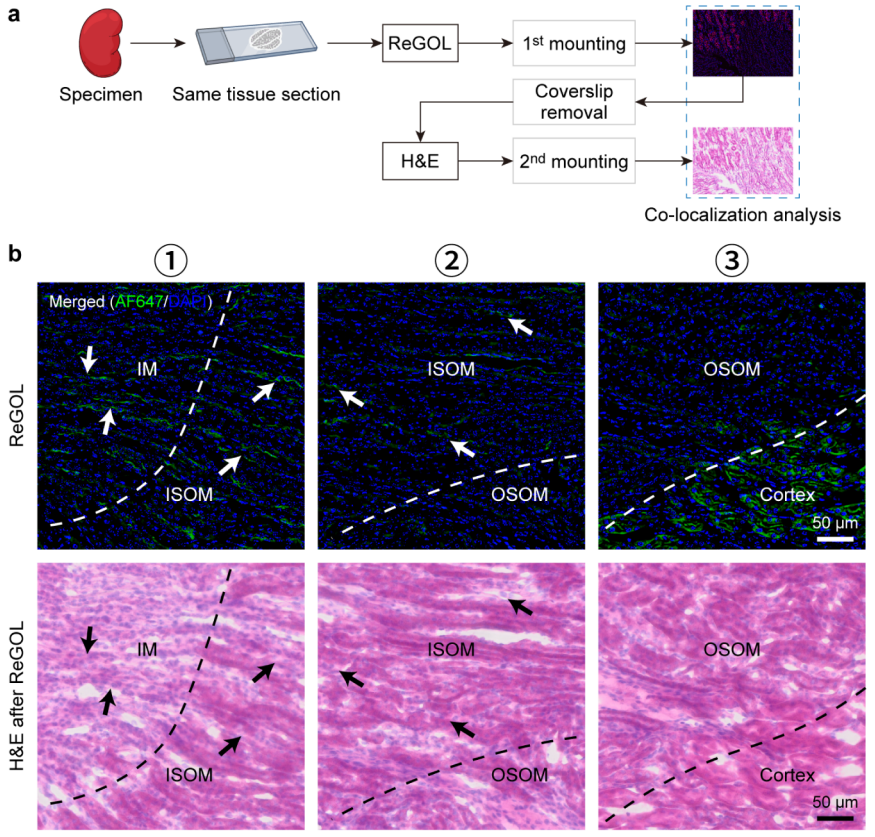

Figure 3. (a) Workflow for ReGOL-Histomap. (b) Scanned images of frozen kidney sections (normal mice) subjected to ReGOL (top, using AF647-Hz as the hydrazide probe) and subsequent H&E staining (bottom). Dashed lines indicate the boundaries of different regions. These are the enlarged views of Figure S13. AF647, labeling signal; DAPI, nuclei. IM, inner medulla; ISOM, inner stripe of the outer medulla; OSOM, outer stripe of the outer medulla. Scale bars, 50 μm. n = 3. White and black arrows indicate the same location.

variations in terminal Gal/GalNAc abundance in tissues. Although this validation supports its use in tissue sections, potential influences on GAO reactivity and hydrazone formation efficiency should be taken into account in more complex biological systems.

Because formalin-fixed paraffin-embedded (FFPE) sections are among the most widely used long-term archival formats in pathology, we further evaluated ReGOL on paraffin-embedded kidney sections. Similar to the results obtained with frozen sections, fine structural signal patterns were retained while the background remained low (Figure S11).

Taken together, these results show that ReGOL enables robust tissue glycan labeling in both frozen and paraffin-embedded sections, with low background, clear spatial resolution, and a simple operational workflow.

Same-Section ReGOL-Histomap Enables Histology-Guided Assignment of Glycan Signals

While ReGOL revealed distinct glycan distribution patterns across multiple organs, fluorescence labeling alone did not always permit unambiguous assignment of the labeled structures within histologically complex tissues. The kidney provides a representative example, because several tubular components are densely packed within the medulla and may display similar elongated morphologies in fluorescence images. We therefore sought to establish a same-section workflow that directly correlates ReGOL signals with conventional histological landmarks.

Previous studies have shown that immunofluorescence (or immunohistochemistry) and hematoxylin and eosin (H&E) staining can be sequentially performed or integrated on the same tissue section, thereby enabling direct comparison between molecular readouts and histological architecture.[30,31] Since ReGOL does not require dehydration or permanent mounting prior to image acquisition, it remains compatible with subsequent H&E staining. Accordingly, we established a sequential same-section workflow, termed ReGOL-HistoMap, in which ReGOL imaging was followed by H&E staining on the identical tissue section (Figure 3a).

When applied to normal kidney sections, this workflow showed that Gal/GalNAc signals were mainly localized to the inner stripe of the outer medulla (ISOM) and the inner medulla (IM) (see Figure S12 for regional anatomy and Figure S13 for imaging data). Comparison with the corresponding H&E images indicated that these signals were not associated with the larger collecting ducts, but more likely with Henle's loops (Figure 3b). We thus infer that these tubular elements were relatively enriched in terminal Gal/GalNAc under the present labeling conditions.

These results demonstrate that same-section integration of ReGOL with H&E staining enables direct correlation between glycan labeling patterns and tissue histology. Rather than serving solely as a confirmatory imaging step, this workflow improves the interpretability of tissue glycan maps by linking molecular glycan information to the histological structures on the same section. This feature may be particularly useful in structurally crowded tissues and in pathological specimens, where accurate assignment of molecular signals is essential.[32]

https://doi.org/10.1021/acs.analchem.6c02366
Anal. Chem. 2026, 98, 20531−20541

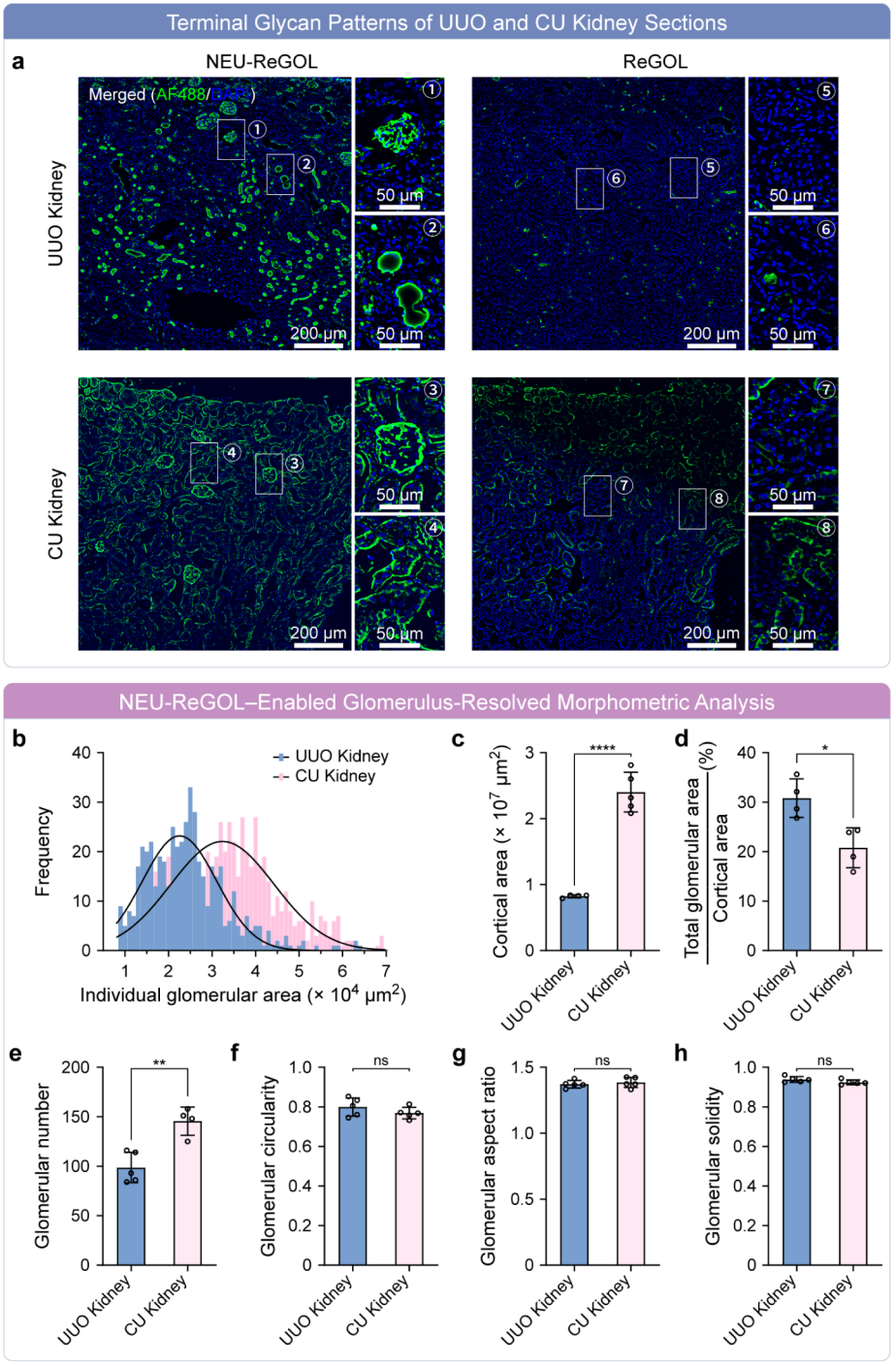

Figure 4. NEU-ReGOL resolves terminal and sialylated Gal/GalNAc in frozen kidney sections and reveals their disease-associated redistribution. (a) Scanned images of frozen sections of UUO and CU kidneys after NEU-ReGOL or ReGOL treatment (using AF488-Hz as the hydrazide probe). AF488, labeling signal; DAPI, nuclei. Insets 1, 3, 5, and 7 indicate glomeruli. Insets 2, 4, 6, and 8 indicate tubules. n = 5. (b–h) NEU-ReGOL–enabled glomerulus-resolved morphometric analysis. (b) Frequency histogram of individual glomerular area. (c) Cortical area. (d) Total glomerular area as a fraction of cortical area. (e) Glomerular number. (f) Glomerular circularity. (g) Glomerular aspect ratio. (h) Glomerular solidity. Data were derived from the representative images shown in (a) and presented as mean ± SD. Statistical significance was calculated via unpaired two-tailed t-test; ****P < 0.0001; **P < 0.01; *P < 0.05; ns, not significant.

NEU-ReGOL Resolves Terminal Gal/GalNAc and Their Sialylated Counterparts in Tissue Sections

Besides Gal/GalNAc, Sia represents another major class of terminal glycans and plays important roles in cell recognition and immune regulation.[33] In cellular samples, selective oxidation of Sia can be achieved by tuning $NaIO_4$ concentration and reaction conditions.[34] In tissue sections, however, Sia is more commonly visualized by periodic acid–Schiff (PAS) staining.[35] Because vicinal diols are widely distributed among tissue glycoconjugates, PAS staining provides limited specificity for Sia.

To address this limitation, we used NEU to selectively remove terminal Sia and combined this step with ReGOL to

https://doi.org/10.1021/acs.analchem.6c02366
Anal. Chem. 2026, 98, 20531−20541

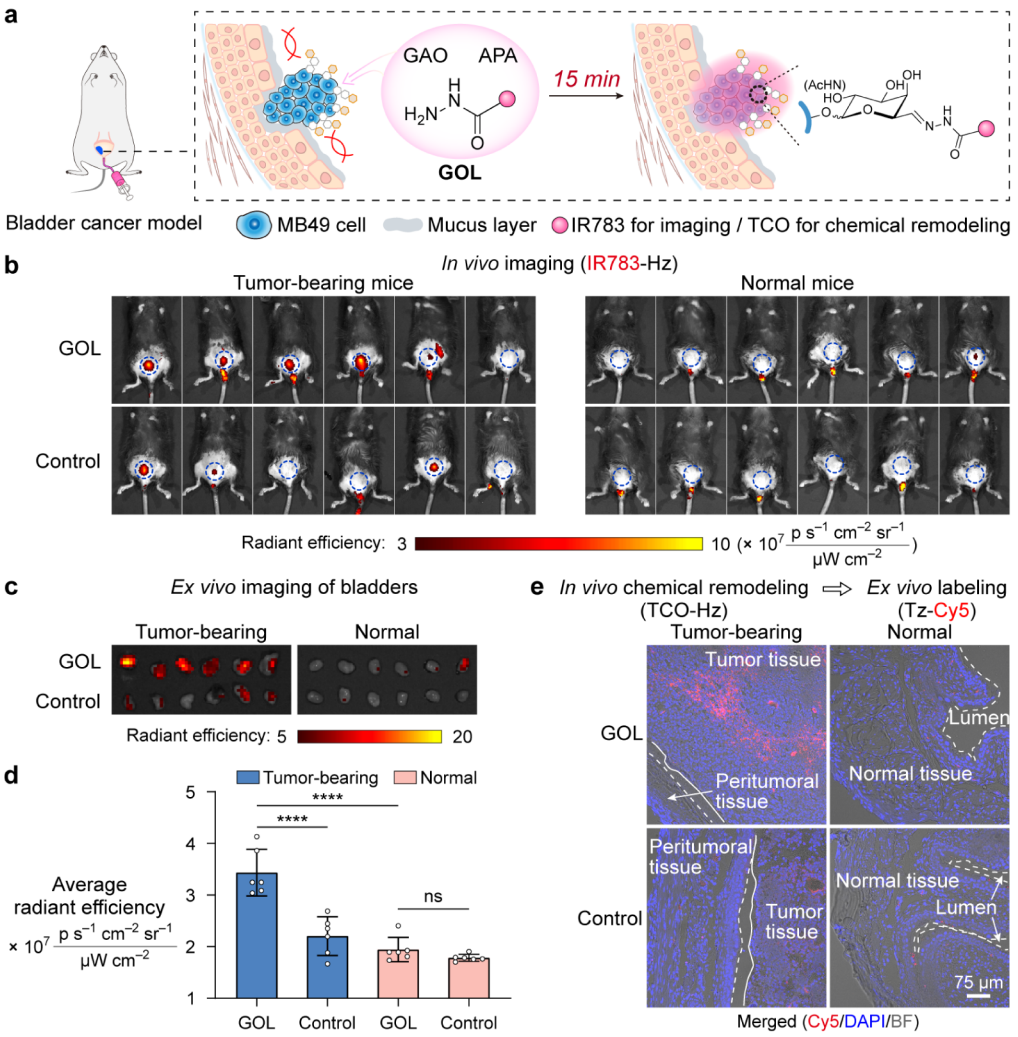

Figure 5. Bladder tumor glycan imaging and chemical engineering in vivo. (a) Schematic illustration of the mechanism of GOL in the tumor-bearing bladder. (b) In vivo imaging of tumor-bearing and normal mice after GOL (using IR783-Hz as the hydrazide probe) or control treatment (IR783-Hz alone). The dashed circles refer to the location of the bladders. $n = 6$ for each group. In vivo bioluminescent imaging confirmed the tumor formation (Figure S17). The experiments were repeated three times with similar results. (c) Ex vivo imaging of the bladders in (b). The unit is the same as in (b). (d) Quantification of the average radiant efficiency in (c). Fluorescence signals were measured using square ROIs that fully enclosed each bladder to ensure consistent analysis across samples. Data were presented as mean ± SD. Statistical significance was calculated via one-way ANOVA followed by Tukey's post hoc test; ****$P < 0.0001$; ns, not significant. (e) In vivo chemical remodeling of bladder tumors. Tumor-bearing and normal mice were subjected to GOL (using TCO-Hz as the hydrazide probe) or control treatment (TCO-Hz alone). $n = 6$ for each group. The bladders in each group were harvested for frozen sectioning for further Tz-Cy5 labeling and CLSM imaging (20×). Cy5 and DAPI indicate the remodeling sites and nuclei, respectively. Scale bar, 75 μm. In tumor-bearing bladder tissues, dashed lines indicate the apical surface of the peritumoral urothelium, and solid lines indicate the tumor margins; in normal bladder tissues, dashed lines indicate the apical surface of the normal urothelium.

establish a NEU-ReGOL workflow. By comparing the signals obtained with ReGOL and NEU-ReGOL, terminal Gal/GalNAc and their sialylated counterparts, typically capped by α2,3- or α2,6-linked Sia, can be resolved in situ. This strategy is conceptually related to NEU-assisted galactose oxidase−Schiff staining procedures,[20] but leverages rapid hydrazone ligation to streamline the workflow and minimizes background interference. In normal kidney sections, NEU-ReGOL produced strong and selective labeling of glomeruli, whereas ReGOL alone gave negligible signals in these structures, indicating that Gal/GalNAc in glomeruli is largely masked by Sia (Figure S14). This result is consistent with prior studies showing pronounced glomerular sialylation in the kidney and the importance of sialylated glycans for glomerular barrier integrity.[36]

We next applied the ReGOL/NEU-ReGOL workflow to a unilateral ureteral obstruction (UUO) model of renal fibrosis[37,38] (14 days postsurgery) to track disease-associated changes in terminal glycan patterns in situ. Masson's trichrome staining revealed marked collagen deposition[39] in the UUO kidneys, validating successful model establishment (Figure S15). Comparative analysis of the UUO kidneys and contralateral unobstructed (CU) kidneys revealed several notable features in the cortex (Figure 4a). First, NEU-ReGOL showed prominent glomerular labeling in both UUO and CU kidneys (insets 1 and 3). Second, in CU kidneys, tubules displayed weak ReGOL signals but pronounced NEU-ReGOL labeling (insets 4 and 8), indicating that Gal/GalNAc in these tubular regions was largely capped by Sia. Third, in UUO kidneys, the labeling pattern of renal tubules was less

https://doi.org/10.1021/acs.analchem.6c02366
Anal. Chem. 2026, 98, 20531−20541

distinct than in CU kidneys (insets 2 and 4), and abundant round-shaped regions with elevated NEU-ReGOL signals were observed (insets 2 and 6). For the latter, their morphology and localization suggest that these structures may correspond to intratubular casts,[40] which are commonly associated with tubular injury in obstructive nephropathy. Together, these observations suggest that renal fibrosis is accompanied not only by changes in terminal glycan abundance, but also by redistribution of terminal glycan presentation across distinct cortical substructures.

Taking advantage of the high-contrast delineation of glomeruli by NEU-ReGOL on kidney sections, we next performed glomerulus-resolved morphometric analysis. The glomerular cross-sectional area was overall reduced in UUO kidneys (Figure 4b). However, because renal fibrosis was accompanied by marked cortical shrinkage (Figures 4c, S15), the relative glomerular area fraction increased by 48% (Figure 4d). Meanwhile, the glomerular number decreased by 32% (Figure 4e), consistent with nephron loss during fibrosis.[41] Morphometric parameters including circularity, aspect ratio, and solidity showed no significant differences between UUO and CU kidneys (Figure 4f–h), indicating that although glomeruli became fewer and smaller, their overall morphology remained relatively preserved at this stage.

Collectively, NEU-ReGOL used in conjunction with ReGOL facilitates the spatially resolved comparison of two terminal glycans in tissue sections. This paired workflow captures how terminal glycan presentation shifts across tissue structures and disease states. Its compatibility with histological morphometry further suggests utility for structure-aware and potentially automated analysis of glycan features in renal pathology.[42,43]

Glycan Imaging-Enabled Delineation of Bladder Tumor Boundaries

In bladder cancer, altered glycosylation is a common molecular feature associated with malignant transformation.[44,45] Aberrant expression of truncated *O*-glycans, including Tn antigen, T antigen, and their sialylated counterparts, has been frequently linked to bladder tumor progression and aggressiveness.[46] To assess whether ReGOL could provide histologically relevant information in bladder cancer, we established an orthotopic mouse bladder tumor model by intravesical inoculation of MB49-luc cells and applied ReGOL to frozen sections obtained from tumor-bearing and normal bladders (Figure S16). ReGOL signals were markedly stronger in tumor tissues than in peritumoral regions, whereas the latter showed signal levels comparable to those in normal urothelium. This signal contrast enabled clear differentiation between tumor and normal tissues, as well as delineation of the tumor–peritumoral-urothelium interface. Differences in cell morphology and spatial organization between tumor cells and adjacent urothelial cells were also observed, further supporting the histological distinction between these regions.

These results indicate that ReGOL can visualize spatial glycan heterogeneity across bladder tumor and nontumor compartments on tissue sections. These findings support the utility of terminal glycan imaging as a tissue-contrast readout for identifying tumor-associated regions. Given that ReGOL on frozen sections requires ~23 min, this workflow may be compatible with future fluorescence-assisted or frozen section-based intraoperative pathological assessment.[47]

In Vivo GOL for Bladder Glycan Imaging and Chemical Remodeling

We next explored whether the 15 min GOL workflow could be translated to in vivo bladder labeling (Figure 5a). MB49-luc-bearing mice (Figure S17) and normal mice were used as models, and a hydrazide-modified near-infrared fluorescent probe, IR783-Hz, was employed for hydrazone ligation. In tumor-bearing mice, the GOL group showed stronger fluorescence signals in the bladders than the control group receiving IR783-Hz alone (Figure 5b). In normal mice, both groups exhibited minimal fluorescence intensity. Ex vivo fluorescence imaging and quantitative analysis of the corresponding bladders further corroborated the in vivo results (Figure 5c,d). We also imaged frozen bladder sections from both experimental groups (Figure S18). IR783 fluorescence was predominantly localized to tumor tissues, whereas minimal signal was observed in normal bladders, consistent with the results in Figure S16.

To better understand the origin of this in vivo signal contrast, we next investigated factors that might influence labeling efficiency, particularly the tissue permeability of the labeling reagents. To this end, GAO was replaced with Cy5-conjugated GAO (GAO-Cy5), and the distributions of GAO-Cy5 and IR783-Hz were examined in bladders that were not rinsed after GOL treatment (Figure S19). In tumor-bearing bladders, both GAO-Cy5 and IR783-Hz penetrated deeply into the tumor regions, whereas their penetration into the peritumoral urothelium was more limited. These observations suggest that the urothelial mucus or glycosaminoglycan layer may hinder reagent access (Figure 5a).[48,49] In normal bladders, GAO-Cy5 showed minimal tissue penetration, whereas IR783-Hz remained detectable (Figure S19). These findings suggest that the signal differences between tumor-bearing and normal mice likely reflected the combined contributions of Gal/GalNAc availability and tissue permeability. Therefore, when translating cell-surface labeling chemistry to in vivo settings, both reaction chemistry and local tissue accessibility must be taken into account. In addition, the in vivo biocompatibility of APA and GOL treatment was evaluated by H&E staining, which revealed no evident tissue damage under the tested conditions (Figure S20). Collectively, these results show that the 15 min GOL workflow enables preferential glycan labeling of bladder tumor tissue in vivo, suggesting potential compatibility with future rapid intraoperative assessment of bladder lesions.[50,51]

Finally, to explore the potential of GOL for in vivo chemical remodeling of bladder tumors, IR783-Hz was replaced with a heterobifunctional probe (TCO-Hz) containing both *trans*-cyclooctene (TCO) and hydrazide groups. TCO-Hz was selected because TCO–tetrazine ligation proceeds with exceptionally rapid kinetics (up to 10^6 M^{-1} s^{-1})[52,53] and has been successfully used in vivo.[54,55] We performed in vivo GOL using TCO-Hz as the hydrazide probe in tumor-bearing and normal mice, collected bladders, and then stained the obtained bladder sections with a Cy5-modified methyltetrazine probe (Tz-Cy5) to visualize the installed TCO handles. As shown in Figure 5e, this approach enabled selective visualization of tumor tissue, with no significant signal detected in peritumoral or normal tissues. Collectively, these findings support GOL as a strategy for localized chemical installation on the tumor glycocalyx in vivo, providing a foundation for future functional remodeling of bladder tumor surfaces.

https://doi.org/10.1021/acs.analchem.6c02366
Anal. Chem. 2026, 98, 20531−20541

CONCLUSIONS

In this work, we developed a Gal/GalNAc labeling platform for tissue section and in vivo glycan analysis. It addresses key challenges inherent to glycan labeling in complex biological systems, particularly the suppression of fixation-derived background, efficient covalent readout under biocompatible conditions, and workflow compatibility across tissue and in vivo settings. At the tissue level, ReGOL demonstrates high fidelity and compatibility with both frozen and paraffin-embedded sections. Integration with H&E staining provides a practical platform for correlating glycan information with histological features. We also developed a comparative NEU-ReGOL/ReGOL strategy to resolve exposed terminal Gal/GalNAc and Sia-capped counterparts. This approach enables morphometric analysis of glomeruli in a renal fibrosis model. In a bladder cancer model, ReGOL enables precise delineation of tumor−peritumoral-urothelium boundaries at the tissue section level, while GOL further supports tumor-selective glycan imaging and localized chemical installation in vivo.

Collectively, this work establishes a practical oxidation-based framework for converting terminal glycan presentation into spatially resolved covalent signals across different section types and disease contexts. Its compatibility with histological analysis and in vivo chemical installation may also facilitate future integration with computational image analysis for structure-aware tissue profiling.[56,57] More broadly, our results highlight glycan-informed analytical strategies as valuable complements to existing histological and molecular approaches for studying complex biological systems.

ASSOCIATED CONTENT

Supporting Information

The Supporting Information is available free of charge at https://pubs.acs.org/doi/10.1021/acs.analchem.6c02366.

Reagents and materials, apparatus, additional experimental details, and supplementary figures (PDF)

AUTHOR INFORMATION

Corresponding Authors

Jian He − *Department of Nuclear Medicine, Nanjing Drum Tower Hospital, Affiliated Hospital of Medical School, Nanjing University, Nanjing 210008, China*; Email: hjxueren@126.com

Pengchao Li − *Department of Urology, The First Affiliated Hospital with Nanjing Medical University, Nanjing 210029, China*; Email: superkulian@aliyun.com

Lin Ding − *State Key Laboratory of Analytical Chemistry for Life Science, School of Chemistry, Nanjing University, Nanjing 210023, China*; orcid.org/0000-0001-5381-3484; Email: dinglin@nju.edu.cn

Authors

Haiqi Wang − *State Key Laboratory of Analytical Chemistry for Life Science, School of Chemistry, Nanjing University, Nanjing 210023, China*

Ru Jia − *State Key Laboratory of Pharmaceutical Biotechnology, School of Life Sciences, Nanjing University, Nanjing 210023, China*

Junpeng Xu − *State Key Laboratory of Pharmaceutical Biotechnology, Medical School, Nanjing University, Nanjing 210093, China*; orcid.org/0009-0001-3452-0763

Qi Li − *Department of Pathology, Nanjing Drum Tower Hospital, Affiliated Hospital of Medical School, Nanjing University, Nanjing 210008, China*

Yiran Li − *College of Food Science and Technology, Nanjing Agricultural University, Nanjing 211800, China*

Yunyan Yao − *Institute of Molecular and Cell Biology (IMCB), Agency for Science, Technology and Research (A*STAR), Singapore 138673, Singapore*

Ruiyuan Wang − *State Key Laboratory of Analytical Chemistry for Life Science, School of Chemistry, Nanjing University, Nanjing 210023, China*

Xincheng Kong − *State Key Laboratory of Pharmaceutical Biotechnology, School of Life Sciences, Nanjing University, Nanjing 210023, China*; orcid.org/0009-0008-7650-4711

Yu Zhu − *State Key Laboratory of Analytical Chemistry for Life Science, School of Chemistry, Nanjing University, Nanjing 210023, China*

Chao Yan − *State Key Laboratory of Pharmaceutical Biotechnology, School of Life Sciences and Chemistry and Biomedicine Innovation Center (ChemBIC), ChemBioMed Interdisciplinary Research Center, Nanjing University, Nanjing 210023, China*

Huangxian Ju − *State Key Laboratory of Analytical Chemistry for Life Science, School of Chemistry, Nanjing University, Nanjing 210023, China*; orcid.org/0000-0002-6741-5302

Complete contact information is available at: https://pubs.acs.org/10.1021/acs.analchem.6c02366

Author Contributions

△H.W. and R.J. contributed equally.

Notes

The authors declare no competing financial interest.

ACKNOWLEDGMENTS

This work was supported by the National Natural Science Foundation of China (22574077, 22274073, 22404080) and the State Key Laboratory of Analytical Chemistry for Life Science (5431ZZXM2504).

REFERENCES

(1) de Haan, N.; Nielsen, M. I.; Wandall, H. H. Reading and Writing the Human Glycocode. *Annu. Rev. Biochem.* **2024**, *93*, 529−564.

(2) Dabelsteen, S.; Pallesen, E. M. H.; Marinova, I. N.; Nielsen, M. I.; Adamopoulou, M.; Rømer, T. B.; Levann, A.; Andersen, M. M.; Ye, Z.; Thein, D.; Bennett, E. P.; Büll, C.; Moons, S. J.; Boltje, T.; Clausen, H.; Vakhrushev, S. Y.; Bagdonaite, I.; Wandall, H. H. Essential Functions of Glycans in Human Epithelia Dissected by a CRISPR-Cas9-Engineered Human Organotypic Skin Model. *Dev. Cell* **2020**, *54*, 669−684.

(3) Moremen, K. W.; Tiemeyer, M.; Nairn, A. V. Vertebrate protein glycosylation: Diversity, synthesis and function. *Nat. Rev. Mol. Cell Biol.* **2012**, *13*, 448−462.

(4) Yamakawa, N.; Vanbeselaere, J.; Chang, L.-Y.; Yu, S.-Y.; Ducrocq, L.; Harduin-Lepers, A.; Kurata, J.; Aoki-Kinoshita, K. F.; Sato, C.; Khoo, K.-H.; et al. Systems glycomics of adult zebrafish identifies organ-specific sialylation and glycosylation patterns. *Nat. Commun.* **2018**, *9* (1), 4647.

(5) RodrÍguez, E.; Schetters, S. T. T.; van Kooyk, Y. The tumour glyco-code as a novel immune checkpoint for immunotherapy. *Nat. Rev. Immunol.* **2018**, *18*, 204−211.

(6) Mariño, K. V.; Cagnoni, A. J.; Croci, D. O.; Rabinovich, G. A. Targeting galectin-driven regulatory circuits in cancer and fibrosis. *Nat. Rev. Drug Discovery* **2023**, *22*, 295−316.
(7) Cheng, B.; Tang, Q.; Zhang, C.; Chen, X. Glycan Labeling and Analysis in Cells and In Vivo. *Annu. Rev. Anal Chem.* **2021**, *14*, 363−387.
(8) Griffin, M. E.; Hsieh-Wilson, L. C. Tools for mammalian glycoscience research. *Cell* **2022**, *185*, 2657−2677.
(9) Masullo, L. A.; Almahayni, K.; Pachmayr, I.; Honsa, M.; Heinze, L.; Fritsche, S.; Grabmayr, H.; Jungmann, R.; Möckl, L. Ångström-resolution imaging of cell-surface glycans. *Nat. Nanotechnol.* **2025**, *20*, 1457−1463.
(10) Wu, Y.; Yang, M.; Xu, Y.; Jia, L.; Li, J.; Wang, X.; Zhao, J.; Cai, Y.; Zhang, Y.; Sun, S. A comprehensive *N*-glycoproteome atlas reveals tissue-specific glycan remodeling but non-random structural micro-heterogeneities. *Nat. Commun.* **2026**, *17* (1), 1448.
(11) Wang, H.; Mooney, D. J. Metabolic glycan labelling for cancer-targeted therapy. *Nat. Chem.* **2020**, *12*, 1102−1114.
(12) Brooks, S. A.; Hall, D. M. S. Lectin Histochemistry to Detect Altered Glycosylation in Cells and Tissues. In *Metastasis Research Protocols*, 2nd ed., Dwek, M.; Brooks, S. A.; Schumacher, U. Eds.; Humana Press, 2012, pp. 31−50.
(13) Rebelo, A. L.; Contessotto, P.; Joyce, K.; Kilcoyne, M.; Pandit, A. An optimized protocol for combined fluorescent lectin/immunohistochemistry to characterize tissue-specific glycan distribution in human or rodent tissues. *STAR Protoc.* **2021**, *2*, 100237.
(14) Cummings, R. D.; Etzler, M.; Hahn, M. G.; Darvill, A.; Godula, K.; Woods, R. J.; Mahal, L. K. Glycan-Recognizing Probes as Tools. In *Essentials of Glycobiology*, 4th ed., Varki, A.; Cummings, R. D.; Esko, J. D.; Stanley, P.; Hart, G. W.; Aebi, M.; Mohnen, D.; Kinoshita, T.; Packer, N. H.; Prestegard, J. H., Eds.; Cold Spring Harbor Laboratory Press, 2022.
(15) Bojar, D.; Meche, L.; Meng, G.; Eng, W.; Smith, D. F.; Cummings, R. D.; Mahal, L. K. A Useful Guide to Lectin Binding: Machine-Learning Directed Annotation of 57 Unique Lectin Specificities. *ACS Chem. Biol.* **2022**, *17*, 2993−3012.
(16) Aguilar, A. L.; Meng, L.; Hou, X.; Li, W.; Moremen, K. W.; Wu, P. Sialyltransferase-Based Chemoenzymatic Histology for the Detection of *N*- and *O*-Glycans. *Bioconjugate Chem.* **2018**, *29* (4), 1231−1239.
(17) Li, Y.; Wang, H.; Chen, Y.; Ding, L.; Ju, H. In Situ Glycan Analysis and Editing in Living Systems. *JACS Au* **2024**, *4*, 384−401.
(18) Schulte, B. A.; Spicer, S. S. Light Microscopic Histochemical Detection of Terminal Galactose and *N*-Acetylgalactosamine Residues in Rodent Complex Carbohydrates Using a Galactose Oxidase−Schiff Sequence and Peanut Lectin−Horseradish Peroxidase Conjugate. *J. Histochem. Cytochem.* **1983**, *31*, 19−24.
(19) Zhu, W.; Zhou, Y.; Guo, L.; Feng, S. Biological function of sialic acid and sialylation in human health and disease. *Cell Death Discovery* **2024**, *10*, 415.
(20) Roberts, G. P.; Gupta, S. K. Use of Galactose Oxidase in the Histochemical Examination of Mucus-secreting Cells. *Nature* **1965**, *207*, 425−426.
(21) Xu, L.; Zhong, T.; Zhao, W.; Yao, B.; Ding, L.; Ju, H. Chemoselective labeling-based spermatozoa glycan imaging reveals abnormal glycosylation in oligoasthenotspermia. *Chin. Chem. Lett.* **2024**, *35*, 108760.
(22) Albrecht, N. E.; Jiang, D.; Akhanov, V.; Hobson, R.; Speer, C. M.; Robichaux, M. A.; Samuel, M. A. Rapid 3D-STORM imaging of diverse molecular targets in tissue. *Cell Rep. Methods* **2022**, *2*, 100253.
(23) Kölmel, D. K.; Kool, E. T. Oximes and Hydrazones in Bioconjugation: Mechanism and Catalysis. *Chem. Rev.* **2017**, *117*, 10358−10376.
(24) Yang, J.; Zhu, B.; Ran, C. The Application of Bio-orthogonality for In Vivo Animal Imaging. *Chem. Biomed. Imaging* **2023**, *1*, 434−447.
(25) Chen, D.; Lin, Y.; Fan, Y.; Li, L.; Tan, C.; Wang, J.; Lin, H.; Gao, J. Glycan Metabolic Fluorine Labeling for In Vivo Visualization of Tumor Cells and In Situ Assessment of Glycosylation Variations. *Angew. Chem.* **2023**, *135*, No. e202313753.
(26) Pinho, S. S.; Torres, J.; Colombel, J.-F. Mucosal glycans: Key drivers of the development of inflammatory bowel disease and a potential new therapeutic target. *Nat. Rev. Gastroenterol. Hepatol.* **2026**, *23*, 318−330.
(27) Wang, H.; Wang, L.; Li, Y.; Cheng, S.; Yao, Y.; Wang, R.; Xu, L.; Kong, D.; Wang, X.; Ding, L.; Ju, H.Kinetic insights underpinning rapid live-cell hydrazone bioconjugation enable in situ quantitative glycan analysis. *Sci. China: Chem.* 2026. .
(28) Kovaříková, P.; Mrkvičková, Z.; Klimeš, J. Investigation of the stability of aromatic hydrazones in plasma and related biological material. *J. Pharm. Biomed. Anal.* **2008**, *47*, 360−370.
(29) Atkins, P.; de Paula, J.; Keeler, J. *Atkins' Physical Chemistry*, 12th ed.; Oxford University Press, 2023, p 763.
(30) Lin, J.-R.; Chen, Y.-A.; Campton, D.; Cooper, J.; Coy, S.; Yapp, C.; Tefft, J. B.; McCarty, E.; Ligon, K. L.; Rodig, S. J.; et al. High-plex immunofluorescence imaging and traditional histology of the same tissue section for discovering image-based biomarkers. *Nat. Cancer* **2023**, *4*, 1036−1052.
(31) Morrison, L. E.; Larrinaga, T. M.; Kelly, B. D.; Lefever, M. R.; Beck, R. C.; Bauer, D. R. Concurrent Viewing of H&E and Multiplex Immunohistochemistry in Clinical Specimens. *Diagnostics* **2025**, *15*, 164.
(32) Enninful, A.; Zhang, Z.; Klymyshyn, D.; Ingalls, M.; Yang, M.; Zong, H.; Bai, Z.; Farzad, N.; Su, G.; Baysoy, A.et al.Integration of imaging-based and sequencing-based spatial omics mapping on the same tissue section via DBiTplus. *Nat. Methods* 2026. DOI: 10.1038/s41592-025-02948-0
(33) Reily, C.; Stewart, T. J.; Renfrow, M. B.; Novak, J. Glycosylation in health and disease. *Nat. Rev. Nephrol.* **2019**, *15*, 346−366.
(34) Zeng, Y.; Ramya, T. N. C.; Dirksen, A.; Dawson, P. E.; Paulson, J. C. High-efficiency labeling of sialylated glycoproteins on living cells. *Nat. Methods* **2009**, *6*, 207−209.
(35) Culling, C. F. A.; Reid, P. E.; Dunn, W. L. A new histochemical method for the identification and visualization of both side chain acylated and nonacylated sialic acids. *J. Histochem. Cytochem.* **1976**, *24*, 1225−1230.
(36) Drake, R. R.; McDowell, C.; West, C.; David, F.; Powers, T. W.; Nowling, T.; Bruner, E.; Mehta, A. S.; Angel, P. M.; Marlow, L. A.; et al. Defining the human kidney N-glycome in normal and cancer tissues using MALDI imaging mass spectrometry. *J. Mass Spectrom.* **2020**, *55* (4), No. e4490.
(37) Wu, W.-P.; Chang, C.-H.; Chiu, Y.-T.; Ku, C.-L.; Wen, M.-C.; Shu, K.-H.; Wu, M.-J. A reduction of unilateral ureteral obstruction-induced renal fibrosis by a therapy combining valsartan with aliskiren. *Am. J. Physiol.: Renal Physiol.* **2010**, *299*, F929−F941.
(38) Sato, N.; Shiraiwa, K.; Kai, K.; Watanabe, A.; Ogawa, S.; Kobayashi, Y.; Yamagishi-Imai, H.; Utsunomiya, Y.; Mitarai, T. Mizoribine Ameliorates the Tubulointerstitial Fibrosis of Obstructive Nephropathy. *Nephron* **2001**, *89*, 177−185.
(39) Yang, J.; Wang, M.; Zhu, F.; Sun, J.; Xu, H.; Chong Lee Shin, O. L.-S.; Zhao, Z.; Pei, G.; Zhu, H.; Cao, C.; He, X.; et al. Putative endothelial progenitor cells do not promote vascular repair but attenuate pericyte−myofibroblast transition in UUO-induced renal fibrosis. *Stem Cell Res. Ther.* **2019**, *10* (1), 104.
(40) Carlisle, R. E.; Mohammed-Ali, Z.; Lu, C.; Yousof, T.; Tat, V.; Nademi, S.; MacDonald, M. E.; Austin, R. C.; Dickhout, J. G. TDAG51 induces renal interstitial fibrosis through modulation of TGF-β receptor 1 in chronic kidney disease. *Cell Death Dis.* **2021**, *12* (10), 921.
(41) Huang, R.; Fu, P.; Ma, L. Kidney fibrosis: From mechanisms to therapeutic medicines. *Signal Transduction Targeted Ther.* **2023**, *8*, 129.
(42) Cho, S. Y.; Kim, Y.; Park, S.; Paik, J. H.; Chin, H. J.; Park, J. H.; Lee, J. P.; Kim, Y.-J.; Park, S.-H.; Lee, H.-C.; et al. Deep learning-based quantitative analysis of glomerular morphology in IgA

nephropathy whole slide images and its prognostic implications. *Sci. Rep.* **2025**, *15* (1), 23566.
(43) Kannan, S.; Morgan, L. A.; Liang, B.; Cheung, M. G.; Lin, C. Q.; Mun, D.; Nader, R. G.; Belghasem, M. E.; Henderson, J. M.; Francis, J. M.; Chitalia, V. C.; Kolachalama, V. B. Segmentation of Glomeruli Within Trichrome Images Using Deep Learning. *Kidney Int. Rep.* **2019**, *4*, 955−962.
(44) Wilczak, M.; Surman, M.; Przybyło, M. Altered Glycosylation in Progression and Management of Bladder Cancer. *Molecules* **2023**, *28*, 3436.
(45) Martínez-Bosch, N.; Rodriguez-Vida, A.; Juanpere, N.; Lloreta, J.; Rovira, A.; Albanell, J.; Bellmunt, J.; Navarro, P. Galectins in prostate and bladder cancer: Tumorigenic roles and clinical opportunities. *Nat. Rev. Urol.* **2019**, *16*, 433−445.
(46) Tan, Z.; Jiang, Y.; Liang, L.; Wu, J.; Cao, L.; Zhou, X.; Song, Z.; Ye, Z.; Zhao, Z.; Feng, H.; et al. Dysregulation and prometastatic function of glycosyltransferase C1GALT1 modulated by cHP1BP3/miR-1-3p axis in bladder cancer. *J. Exp. Clin. Cancer Res.* **2022**, *41*, 228.
(47) Voskuil, F. J.; Vonk, J.; van der Vegt, B.; Kruijff, S.; Ntziachristos, V.; van der Zaag, P. J.; Witjes, M. J. H.; van Dam, G. M. Intraoperative imaging in pathology-assisted surgery. *Nat. Biomed. Eng.* **2022**, *6*, 503−514.
(48) Li, Z.-A.; Wen, K.-C.; Liu, J.-H.; Zhang, C.; Zhang, F.; Li, F.-Q. Strategies for intravesical drug delivery: From bladder physiological barriers and potential transport mechanisms. *Acta Pharm. Sin. B* **2024**, *14*, 4738−4755.
(49) Zhang, P.; Wu, G.; Zhang, D.; Lai, W.-F. Mechanisms and strategies to enhance penetration during intravesical drug therapy for bladder cancer. *J. Controlled Release* **2023**, *354*, 69−79.
(50) Nguyen, Q. T.; Tsien, R. Y. Fluorescence-guided surgery with live molecular navigation—a new cutting edge. *Nat. Rev. Cancer* **2013**, *13*, 653−662.
(51) Teranishi, K. In Vivo Optical Imaging of Bladder Cancer Tissues in an MB49 Bladder Cancer Orthotopic Mouse Model Using the Intravesical or Intravenous Administration of Near-Infrared Fluorescence Probe. *Int. J. Mol. Sci.* **2023**, *24*, 2349.
(52) Darko, A.; Wallace, S.; Dmitrenko, O.; Machovina, M. M.; Mehl, R. A.; Chin, J. W.; Fox, J. M. Conformationally strained *trans*-cyclooctene with improved stability and excellent reactivity in tetrazine ligation. *Chem. Sci.* **2014**, *5*, 3770−3776.
(53) Taylor, M. T.; Blackman, M. L.; Dmitrenko, O.; Fox, J. M. Design and Synthesis of Highly Reactive Dienophiles for the Tetrazine−*trans*-Cyclooctene Ligation. *J. Am. Chem. Soc.* **2011**, *133*, 9646−9649.
(54) Neves, A. A.; Stöckmann, H.; Wainman, Y. A.; Kuo, J. C.-H.; Fawcett, S.; Leeper, F. J.; Brindle, K. M. Imaging Cell Surface Glycosylation in Vivo Using "Double Click" Chemistry. *Bioconjugate Chem.* **2013**, *24*, 934−941.
(55) Mao, W.; Dong, P.; Du, W.; Wu, H. Fluorogenic Tetrazine Bioorthogonal Probes for Advanced Application in Bioimaging and Biomedicine. *Chem. Biomed. Imaging* **2025**, *3*, 1−4.
(56) Saldanha, O. L.; Quirke, P.; West, N. P.; James, J. A.; Loughrey, M. B.; Grabsch, H. I.; Salto-Tellez, M.; Alwers, E.; Cifci, D.; Laleh, N. G.; et al. Swarm learning for decentralized artificial intelligence in cancer histopathology. *Nat. Med.* **2022**, *28* (6), 1232−1239.
(57) Liu, T.; Huang, T.; Ding, T.; Wu, H.; Humphrey, P.; Perincheri, S.; Schalper, K.; Ying, R.; Xu, H.; Zou, J.; Mahmood, F.; Zhao, H. Leveraging multi-modal foundation models for analysing spatial multi-omic and histopathology data. *Nat. Biomed. Eng.* 2026. DOI: 10.1038/s41551-025-01602-6.

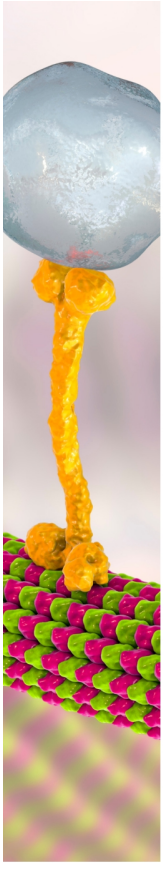

CAS BIOFINDER DISCOVERY PLATFORM™
BRIDGE BIOLOGY AND CHEMISTRY FOR FASTER ANSWERS
Analyze target relationships, compound effects, and disease pathways
Explore the platform
CAS
A division of the American Chemical Society

https://doi.org/10.1021/acs.analchem.6c02366
Anal. Chem. 2026, 98, 20531−20541